The electrocatalytic stereomutation of arylazosulfides. A spectroelectrochemical investigation

ARTICLE *in* JOURNAL OF ELECTROANALYTICAL CHEMISTRY · FEBRUARY 1997

Impact Factor: 2.87 · DOI: 10.1016/S0022-0728(96)04900-5

6 AUTHORS, INCLUDING:

Andreas Neudeck
TITV Greiz
86 PUBLICATIONS **1,062** CITATIONS
SEE PROFILE

Jean Pinson
Paris Diderot University
162 PUBLICATIONS **7,589** CITATIONS
SEE PROFILE

Giovanni Petrillo
Università degli Studi di Genova
146 PUBLICATIONS **1,377** CITATIONS
SEE PROFILE

ELSEVIER

Journal of Electroanalytical Chemistry 422 (1997) 99–114

JOURNAL OF ELECTROANALYTICAL CHEMISTRY

The electrocatalytic stereomutation of arylazosulfides. A spectroelectrochemical investigation

Philippe Hapiot [a], Andreas Neudeck [a,*], Jean Pinson [a], Marino Novi [*, b], Giovanni Petrillo [b], Cinzia Tavani [b]

[a] *Laboratoire d'Electrochimie Moléculaire de l'Université Paris 7, Unité Associée au CNRS no 438, 2 Place Jussieu, F-75251 Paris Cedex 05, France*
[b] *Dipartimento di Chimica e Chimica Indutriale, CNR, Centro di Studio per la Chimica dei Composti Cicloalifatici e Aromatici, Via Dodecaneso 31, I-16146 Genoa, Italy*

Received 31 May 1996; revised 23 July 1996

Abstract

Spectroelectrochemistry using a cell with a short conversion time of about 2 s and fast scan cyclic voltammetry permits us to observe the radical anions of 4-nitro- and 4-cyano-phenylazo *tert*-butyl sulfides and to measure the electrocatalyzed *(Z)* to *(E)* stereomutation. The rate of this fast isomerization is of the order of $10^6\ s^{-1}$. It was also possible to characterize kinetically the photostationary state obtained upon light irradiation.

Keywords: Stereomutation; Arylazosulfides; Spectroelectrochemistry; Electrocatalysis

1. Introduction

Arylazosulfides **1** have recently been exploited for the synthesis of a number of variously functionalized aromatic compounds [1–7]. For this purpose they have been used as substrates in $S_{RN}1$ reactions [8,9] with suitable anionic nucleophiles (Nu^-). The $\mathbf{1}^{\cdot-}$ radical anion, obtained via cathodic or homogeneous reduction (e.g. by the nucleophile itself, sometimes under photostimulation) (reaction (1)) has been proposed to cleave (reaction (2)) to give eventually nitrogen, thiolate and an aryl radical; coupling between $Ar^{\cdot}$ and the nucleophile generates (reaction (3)) the radical anion of the substitution product, which effectively closes the propagation cycle by means of an electron exchange with the substrate (reaction (4)). Anyway, the 'external' nucleophile (Nu^-) always suffers competition from RS^-.

$$\underset{\mathbf{1}}{ArN{=}NSR} + \text{electron donor} \leftrightarrows \underset{\mathbf{1}^{\cdot-}}{ArN{=}NSR^{\cdot-}} \quad (1)$$

$$\underset{\mathbf{1}^{\cdot-}}{ArN{=}NSR^{\cdot-}} \xrightarrow{k_2} Ar^{\cdot} + N_2 + {}^-SR \quad (2)$$

$$Ar^{\cdot} + Nu^- \xrightarrow{k_3} ArNu^{\cdot-} \quad (3)$$

$$ArNu^{\cdot-} + ArN{=}NSR \leftrightarrows ArNu + ArN{=}NSR^{\cdot-} \quad (4)$$

(i.e. the 'internal' nucleophile, formed along the fragmentation step 2), whose coupling with $Ar^{\cdot}$ (reaction (3')) triggers an alternative propagation cycle leading to the ArSR sulfide **2**.

$$Ar^{\cdot} + {}^-SR \xrightarrow{k_{3'}} ArSR^{\cdot-} \quad (3')$$

$$ArSR^{\cdot-} + ArN{=}NSR \leftrightarrows \underset{\mathbf{2}}{ArSR} + ArN{=}NSR^{\cdot-} \quad (4')$$

By means of electrochemistry, which has proved to be a very efficient way of initiating and analysing $S_{RN}1$ processes [10–13], it has been possible, in particular, to demonstrate that reaction (3') can also take place in a solvent cage [14]. As a matter of fact, analysis by cyclic voltammetry of the behavior of arylazosulfides upon cathodic reduction in the presence of increasing amounts of cyanide as the 'external' nucleophile has revealed, at least in some cases, the existence, in the plot of ArCN per cent vs. $[CN^-]$, of a plateau region at high $[CN^-]$ values which are significantly less than 100%; this clearly indicates that a fraction of aryl radicals cannot be trapped by the 'external' nucleophile. Furthermore, it was found that the trapping of the 4-cyanophenyl radical is more efficient starting from *(E)*-4-cyanophenylazo *tert*-butyl sulfide than from the *(Z)*-isomer, although these two compounds present, in the absence of CN^-, the same low scan rate cyclic voltammetry. (The results previously obtained [14] have been revised in the present paper.)

* Corresponding authors.

PII S0022-0728(96)04900-5

Since some *(Z)* to *(E)* stereomutation at the level of radical anion could be expected for azosulfides as for analogous azocompounds [15,16], we undertook a thorough investigation of such possible stereomutation on the 4-nitrophenylazo (**1a**) and 4-cyanophenylazo *tert*-butyl sulfides (**1b**), both under electrochemical and photochemical stimulation.

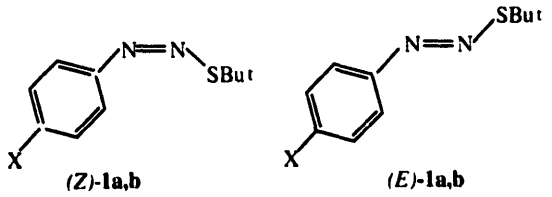

a: X = NO_2 ; b: X = CN

In order to reach this goal, experiments have been performed taking advantage of a recently developed spectroelectrochemical cell equipped with a gold honeycomb structure as an optical transparent electrode (gold–LIGA electrode). Such a very thin cell permits the complete conversion of the substrate in less than 2 s, allowing the observation of intermediates with half-lifetimes between approximately 0.01 s and several minutes [17–19].

2. Experimental

The spectroelectrochemical cell based on a gold–LIGA structure has been described previously [17–19]. The spectra were recorded with a fast scanning (3 ms per spectrum) diode array spectrometer (J. and M. Analytische Mess- und Regeltechnik Gmbh, Aalen, Germany). The 75 W xenon lamp and the spectrophotometer were connected by optical wave guides with the LIGA cell. The reference was an Ag|AgCl electrode standardized against the ferrocene/ferrocenium couple. All the potentials in the text are referred to this couple (E vs. Fc/Fc^+ = E vs. SCE - 0.405 V). In order to minimize photochemical isomerization in the course of the electrochemical experiments (see later), the light intensity was decreased by placing the optical waveguides at a proper distance from the entrance of the cell and keeping the shutter of the spectrophotometer closed between the recording of successive spectra.

Low scan rate cyclic voltammograms were recorded on 1 mm gold or 0.8 mm glassy carbon electrodes using a home-made potentiostat. A home-made program using a

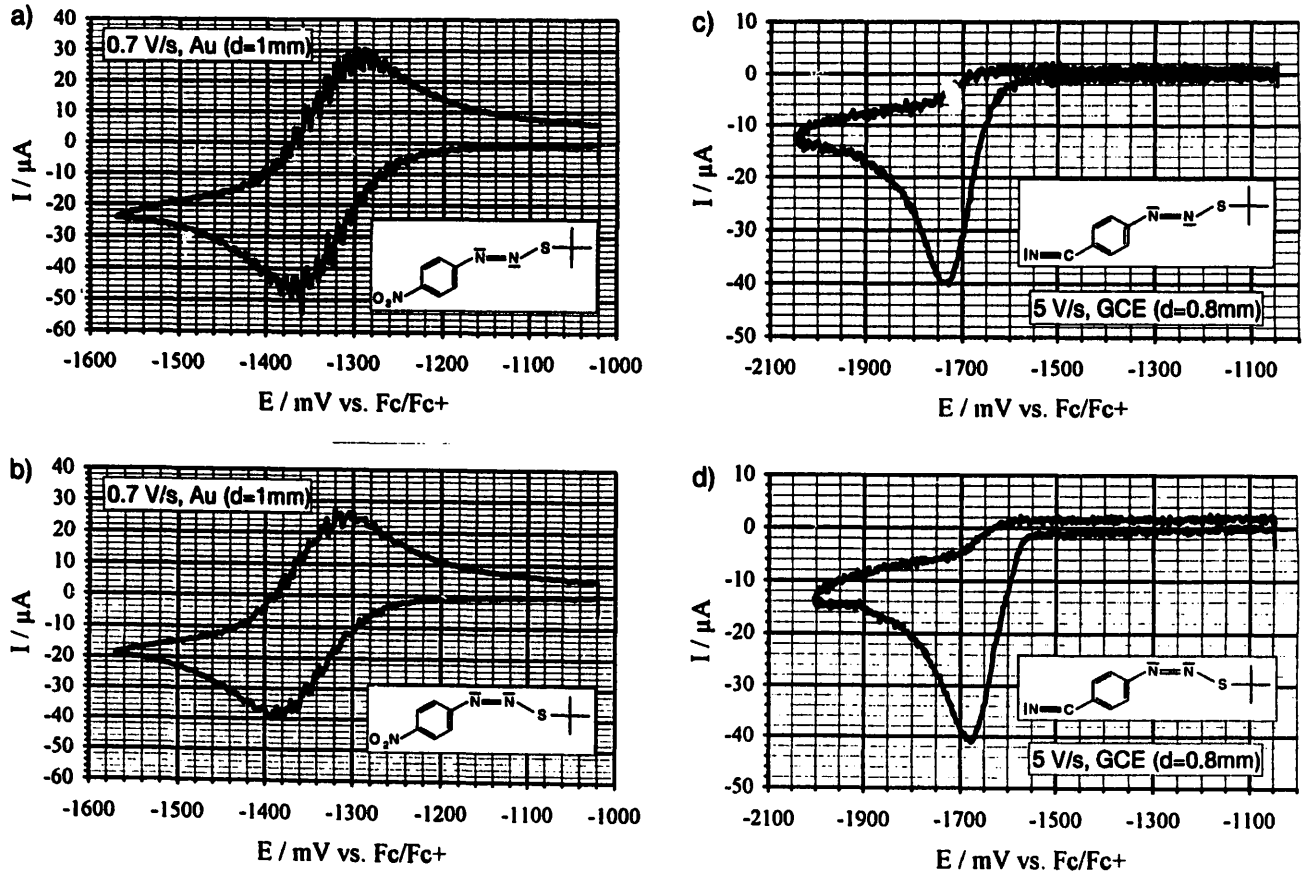

Fig. 1. Cyclic voltammograms of (a) 2.7 mM *(E)*-**1a** and (b) 2.5 mM *(Z)*-**1a** on a 1 mm gold disk electrode at 0.7 $V s^{-1}$ and of (c) 2.8 mM *(E)*-**1b** and (d) 2.6 mM *(Z)*-**1b** on a 0.8 mm glassy carbon disk electrode at 5 $V s^{-1}$. Solvent ACN + 0.1 M NBu_4ClO_4.

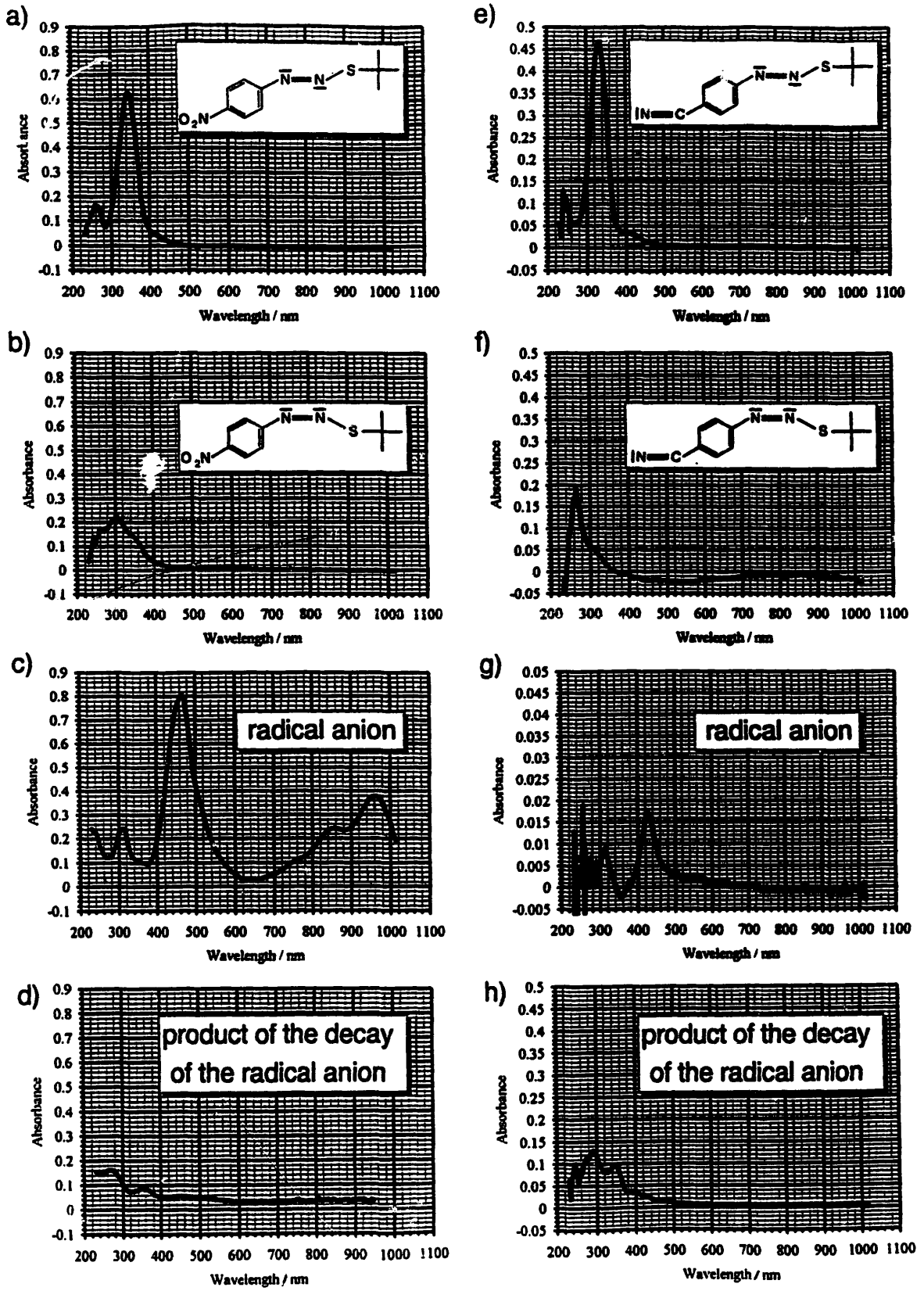

Fig. 2. UV–vis–NIR spectra of (a) 2.4 mM *(E)*-**1a**; (b) 2.4 mM *(Z)*-**1a**; (c) the spectrum of the radical anion $\mathbf{1a}^{\cdot-}$ (2.4 mM) obtained by reduction of either isomer; (d) the product of the decay of $\mathbf{1a}^{\cdot-}$ after 15 min; (e) 2.0 mM *(E)*-**1b**; (f) 1.4 mM *(Z)*-**1b**; (g) the spectrum of the radical anion $\mathbf{1b}^{\cdot-}$ obtained by reduction of *(E)*-**1b** 100 ms after the potential step (cf. Fig. 6); (h) the product of the decay of $\mathbf{1b}^{\cdot-}$ observed by reduction of *(E)*-**1b** as well as *(Z)*-**1b**. Solvent ACN + 0.1 M NBu_4ClO_4.

DA-AD card [17] drove the potentiostat and recorded the current data.

For high scan rate cyclic voltammetry, the microelectrode was a gold wire (10 μm diameter) sealed in soft glass [20]. The signal generator was a Hewlett-Packard 3314A and the curves were recorded using a 4094 Nicolet oscilloscope with a minimum acquisition time of 5 ns per point.

Acetonitrile (0.005% water) and the supporting electrolyte tetrabutylammonium perchlorate were used without further purification. Both *(E)*- and *(Z)*-azosulfides were synthesized as reported previously [3,4,21].

Measurements of the percentage of 4-cyanophenyl radicals trapped by excess of cyanide ions providing a plateau value at high [CN^-] [14] were performed by preparing 10 mM solutions of both isomers of **1b** and concentrated (0.3–0.5 M) solutions of tetraethylammonium cyanide in acetonitrile. Aliquots of these two solutions were diluted with ACN in a volumetric flask containing the proper amount of NBu_4ClO_4 in order to obtain 1 mM solutions **1b** of varying concentrations of CN^- in ACN + 0.1 M NBu_4ClO_4. The voltammograms were then recorded, the height of the wave of **1b** corresponding to twice the percentage of 4-cyanophenyl radicals undergoing further reduction or hydrogen atom abstraction and the height of the wave of terephthalonitrile providing the percentage of 4-cyanophenyl radicals trapped by cyanide ions [14].

3. Results and discussion

3.1. Low scan rate cyclic voltammetry

On a gold electrode, in an acetonitrile (ACN) + 0.1 M NBu_4ClO_4 solution, *(E)*- and *(Z)*-**1a** present similar voltammograms at a scan rate of 0.7 V s^{-1}. For *(E)*-**1a** (Fig. 1(a)) a first reversible (ΔE_p = 61 mV) one-electron wave is located at $E^\circ = -1.33$ V vs. Fc/Fc^+ (−0.92 V vs. SCE), this first wave is followed by a second two-electron irreversible wave (not shown in Fig. 1(a)) at $E_{pc} = -1.99$ V vs. Fc/Fc^+ (−1.58 V vs. SCE). On the reverse sweep, if the second wave has been scanned beforehand, an anodic peak is observed at $E_{pa} = -1.43$ V vs. Fc/Fc^+ (−1.02 V vs. SCE) corresponding to the oxidation wave of the nitrobenzene radical anion as can be ascertained by comparison (cyclic voltammetry or spectroelectrochemistry in the LIGA cell) with an authentic sample of nitrobenzene. Starting from *(Z)*-**1a** (Fig. 1(b)) a practically identical $E^\circ = -1.34$ V vs. Fc/Fc^+ can be determined. The voltammograms of the two isomers remain very simi-

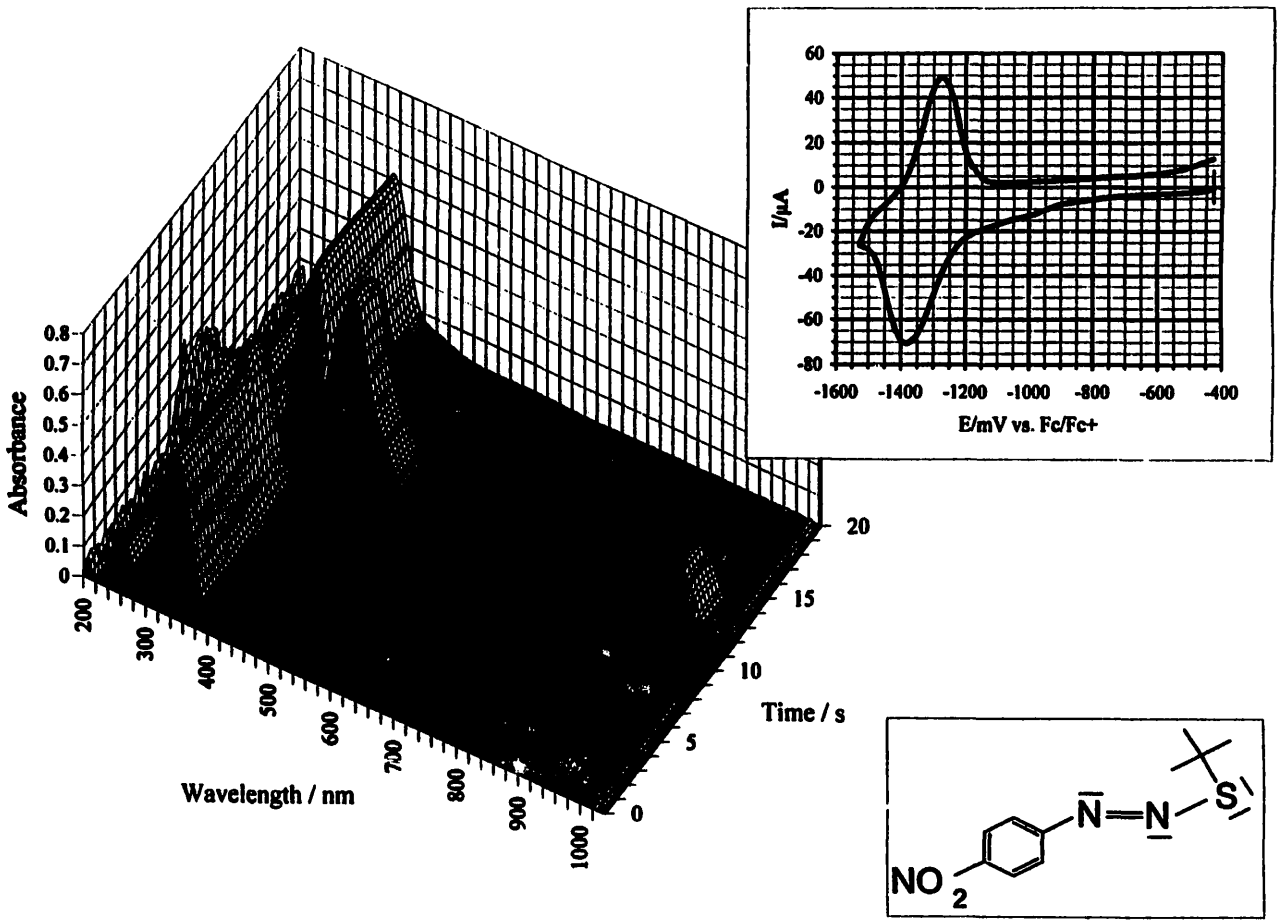

Fig. 3. Absorbance–wavelength–time and current–potential plot of the spectrocyclic voltammogram of 2.2 mM *(E)*-**1a** in ACN + 0.1 M NBu_4ClO_4.

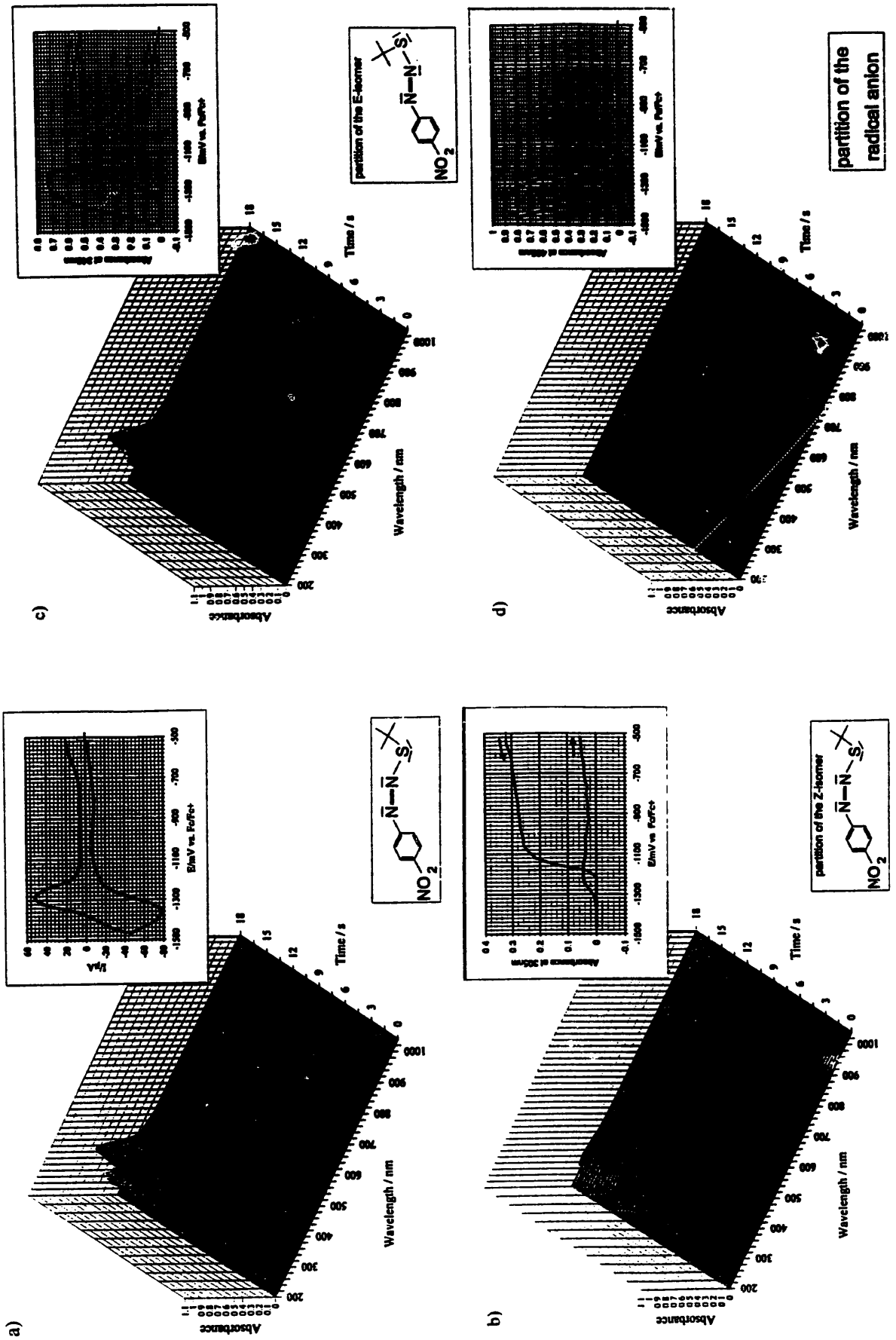

Fig. 4. Absorbance–wavelength–time plots: (a) of (*Z*)-**1a** with the corresponding cyclic voltammogram (in the LIGA cell) and of the numerically separated partitions of (b) (*Z*)-**1a**, (c) (*E*)-**1a** and (d) **1a**$^{\cdot-}$ with their corresponding absorbance–potential curves. Solvent ACN + 0.1 M NBu_4ClO_4.

lar up to a scan rate of 200 $V s^{-1}$, an outcome which can be interpreted in the following way: the stable (on the timescale of the cyclic voltammetry experiment) radical anion **1a**$^{\cdot-}$ is formed at the level of the first wave while the di-anion is obtained at the potential of the second wave; this unstable di-anion eventually cleaves, yielding nitrobenzene which is reduced at the potential where it is formed, therefore leading to the observation of the oxidation wave of the nitrobenzene radical anion on the positive scan.

The voltammograms of *(E)*- and *(Z)*-**1b** on a glassy carbon electrode are also shown in Fig. 1(c) and Fig. 1(d) at a scan rate of 5 $V s^{-1}$. Only minute differences can be seen between the two isomers; the first irreversible wave is located at −1.72 V vs. Fc/Fc^+ (−1.31 V vs. SCE) for *(E)*-**1b** and −1.68 V vs. Fc/Fc^+ for *(Z)*-**1b**. In a previous investigation [14] the height of this wave was measured; it corresponds to the consumption of 0.81 electrons per molecule at 0.2 $V s^{-1}$. It is followed at more negative potentials by the wave of 4-cyanophenyl *tert*-butyl sulfide formed along an $S_{RN}1$ process [14].

Therefore, the low scan rate cyclic voltammetry above does not permit us to differentiate between the electrochemical behavior of *(E)*- and *(Z)*-isomers of both **1a** and **1b**, leaving basically two possibilities open: either there is no stereomutation at the level of the radical anion or this stereomutation is too fast relative to the timescale of the voltammograms.

3.2. Spectroelectrochemistry

Unlike low scan rate cyclic voltammetry, UV–vis spectroscopy allows us to observe a remarkable difference between the *(E)*- and *(Z)*-isomers for both **1a** and **1b** as

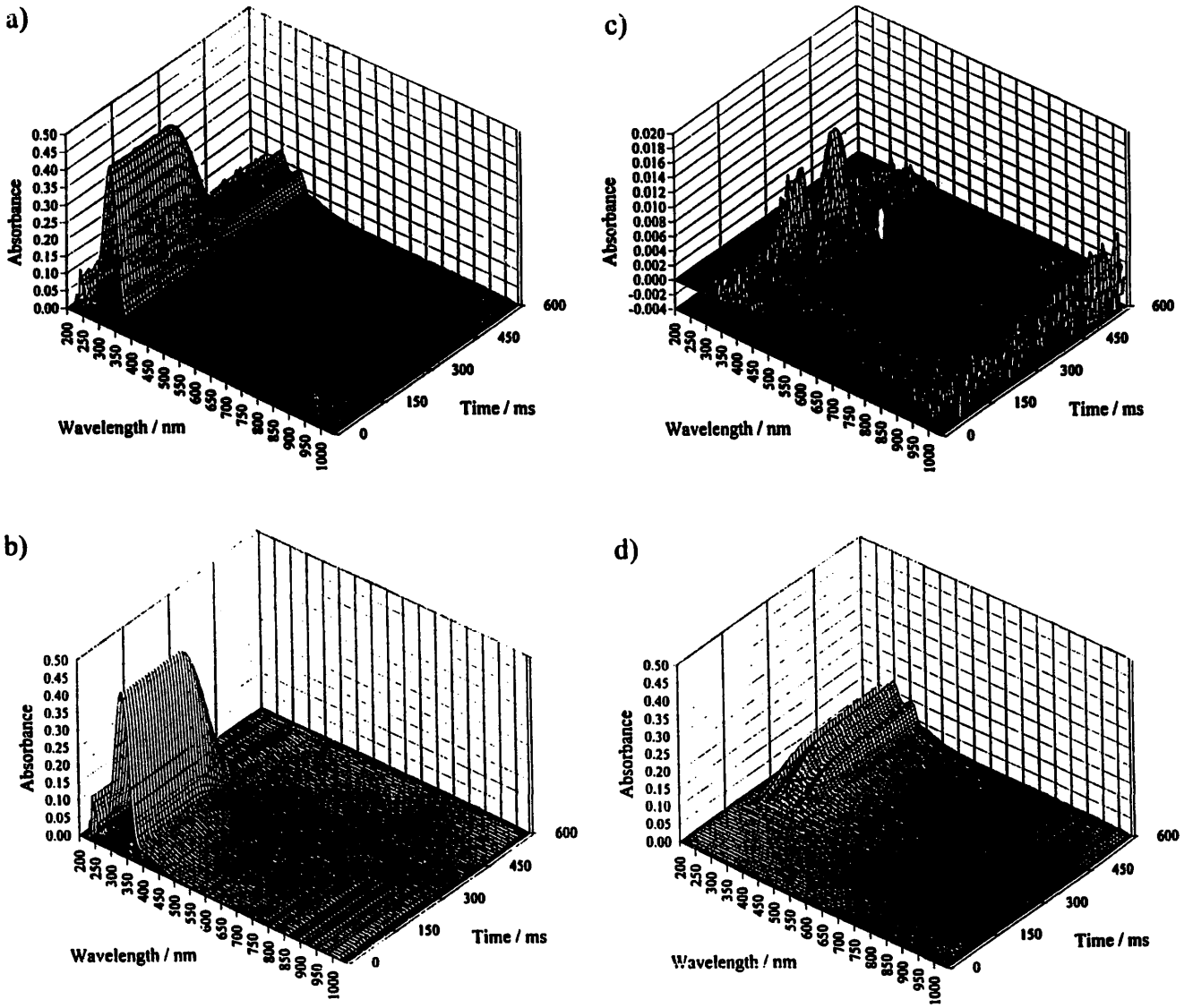

Fig. 5. Spectrochronoamperometry of *(E)*-**1b**, potential step from −1.20 to −1.70 V vs. Fc/Fc^+: (a) recorded spectra; (b) separated spectra of *(E)*-**1b**; (c) separated spectra of **1b**$^{\cdot-}$; (d) separated spectra of the final product 4-cyanophenyl *tert*-butylsulfide. Initial concentration of *(E)*-**1b** 2.0 mM in ACN + 0.1 M NBu_4ClO_4.

shown in Fig. 2; e.g. *(E)*-**1a** (Fig. 2(a)) shows a maximum at 345 nm while *(Z)*-**1a** (Fig. 2(b)) presents a maximum at 305 nm and a shoulder at 345 nm. Similarly, the absorption maximum of *(E)*-**1b** is located at 331 nm (Fig. 2(e)) and the *(Z)*-isomer presents a shoulder at about 300 nm (Fig. 2(f)). Considering **1a**, if the potential of the gold–LIGA electrode is stepped to -1.45 V vs. Fc/Fc^+, i.e. a potential negative to the first wave of **1a**, the same spectrum can be observed starting from the *(Z)*- or the *(E)*-isomer. This spectrum can be assigned to the stable radical anion; λ_{max} 468, 850 and 959 nm with a shoulder at 750 nm (Fig. 2(c)). If after 5 s the potential of the electrode is stepped back to -0.75 V vs. Fc/Fc^+, i.e. a potential positive to the reduction wave of **1a**, the spectrum of *(E)*-**1a** appears whatever the starting isomer. This indicates that at the level of the radical anion one observes a fast conversion of the *(Z)*- to the *(E)*-isomer. After a 15 min electrolysis a new spectrum can be recorded which can be assigned to the 4-nitrophenyl *tert*-butyl sulfide (Fig. 2(d)). Following the decay of $\mathbf{1a}^{\cdot-}$ by spectroscopy it is possible to measure the rate constant of its cleavage, $k_2 = 7.5 \times 10^{-3}\ s^{-1}$ ($t^{1/2} = 92$ s) at room temperature.

Most appealingly, the spectroelectrochemical cell permits us to record at the same time the voltammogram and the UV spectrum. This is shown in the case of *(E)*-**1a** (at $0.11\ V\ s^{-1}$) in Fig. 3 (which also displays the voltammogram in the inset); the intensity of the spectrum of *(E)*-**1a** at 345 nm remains constant to approximately -1.1 V vs. Fc/Fc^+ (at the foot of the cathodic wave) where a small increase [which, as we shall see below, can be attributed to some *(Z)* to *(E)* conversion of a minute amount of the *(Z)*-isomer photochemically formed during the experiment] is observed just before a rapid decrease leading to the spectrum of the $\mathbf{1a}^{\cdot-}$ radical anion. On the reverse, positive scan the spectrum of *(E)*-**1a** is restored.

The outcome (Fig. 4(a)) is quite different when starting from *(Z)*-**1a**. Scanning the potential towards negative values, the spectrum of the *(Z)*-isomer is observed from -0.50 V vs. Fc/Fc^+ to about -1.1 V vs. Fc/Fc^+; at this potential located well in front of the azosulfide reduction

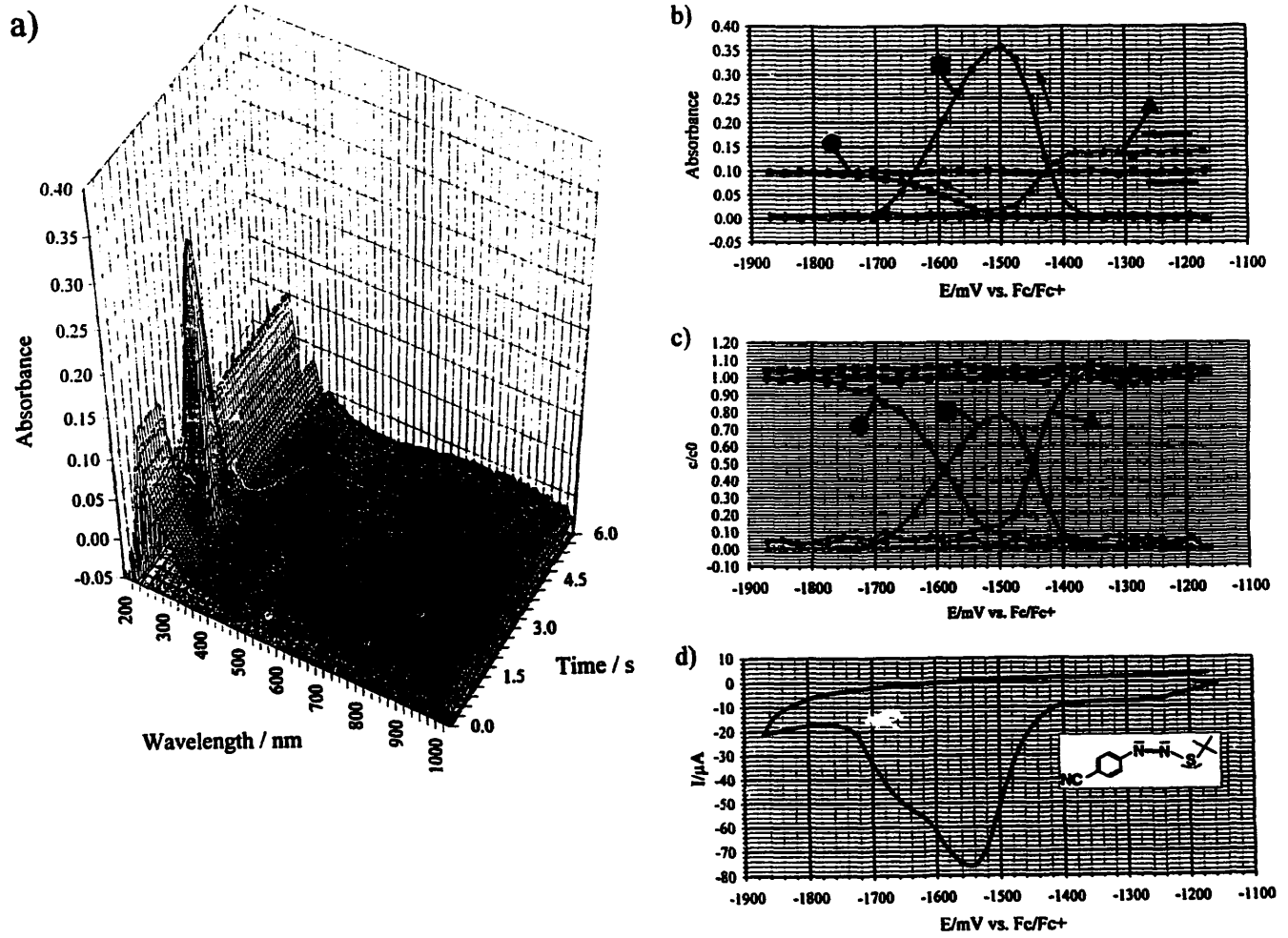

Fig. 6. (a) Spectrocyclic voltammogram of *(Z)*-**1b** on a gold LIGA electrode; (b) the absorbance–potential plot of each species obtained from the numerical separation of the superimposed spectra, ▲ separated *(Z)*-isomer at 266 nm, ◆ separated *(E)*-isomer at 331 nm, ● separated product at 289 nm; (c) the normalized concentration–potential plot and (d) the cyclic voltammogram recorded simultaneously on the same electrode. $c = 1.4$ mM; solvent ACN + 0.1 M NBu_4ClO_4.

wave, a sudden increase of the intensity is observed and the spectrum of *(E)*-**1a** appears. At more negative potentials, the spectrum of the $\mathbf{1a}^{\cdot-}$ radical anion is observed and on the reverse scan *(E)*-**1a** is essentially restored (Fig. 4(a)). This can be confirmed by numerically separating the spectrocyclic voltammogram of Fig. 4(a) into its different components [17–19]: *(Z)*-**1a** is observed up to about -1.1 V vs. Fc/Fc^+ at which potential it suddenly disappears. At this same potential the spectrum of *(E)*-**1a** appears (Fig. 4(c)) before the wave of $\mathbf{1a}/\mathbf{1a}^{\cdot-}$. The formation of the $\mathbf{1a}^{\cdot-}$ radical anion occurs simultaneously with the disappearance of the spectrum of *(E)*-**1a** (Fig. 4(d)). Finally, the separation of the spectra is correct as the remaining spectrum (not shown) is negligible. This is also exemplified in the inset to Fig. 4 which shows the variations of absorbance at the maximum of each of the species as a function of the potential. *(Z)*-**1a** ($\lambda_{max} = 305$ nm) disappears at approximately -1.1 V vs. Fc/Fc^+ while *(E)*-**1a** ($\lambda_{max} = 345$ nm) appears at the same potential. This last species gives place to its radical anion ($\lambda_{max} = 465$ nm) at -1.3 V vs. Fc/Fc^+ and is restored on the reverse scan. This spectrocyclic voltammogram also indicates that even at such a slow scan rate the decomposition of the radical anion does not take place significantly as the spectrum of the 4-nitrophenyl *tert*-butyl sulfide is not observed.

Let us now consider compound *(E)*-**1b**. After a waiting time of 175 ms a potential step from -1.20 to -1.70 V vs. Fc/Fc^+ is applied to the gold–LIGA electrode, the current rises and then decreases while the spectrum (Fig. 5(a)) of *(E)*-**1b** ($\lambda_{max} = 331$ nm) disappears rapidly as can also be observed from the numerically separated spectrum (Fig. 5(b)). An intermediate with a low absorbance can also be detected on the numerically separated spectra; it can be observed for approximately 200 ms (Fig. 5(c)) with an absorption maximum at $\lambda_{max} = 426$ nm (Fig. 2(g)). This spectrum can tentatively be assigned to the radical anion $\mathbf{1b}^{\cdot-}$ and the relevant low absorbance should be attributed to the low concentration of such a frangible species. From the decay of the spectrum, the rate constant (see Appendix A) for the cleavage of the radical anion can be measured as $430 < k_{2[(E)\text{-}\mathbf{1b}]} < 670\ s^{-1}$. At longer times (Fig. 5(d)) the spectrum of the final product ($\lambda_{max} = 292$ and 350 nm)

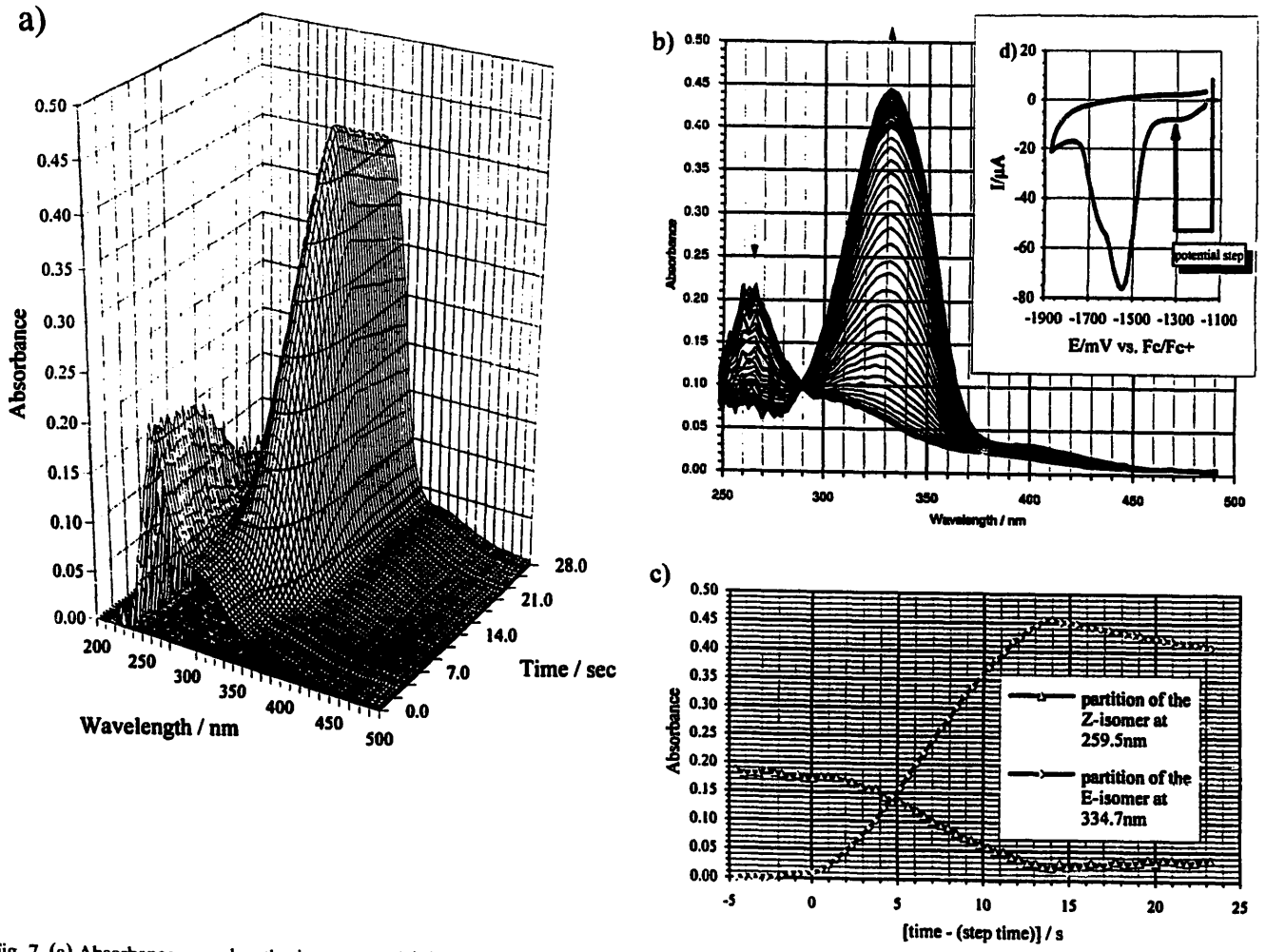

Fig. 7. (a) Absorbance–wavelength–time curve of *(Z)*-**1b** recorded on a gold LIGA electrode, the inset shows (b) the two-dimensional absorbance–wavelength plot with an isosbestic point at 290 nm, (c) the absorbance–time dependence of the *(Z)*- and *(E)*-isomers and (d) the cyclic voltammogram of Fig. 6 to show the potential step corresponding to the current in the cyclic voltammogram. $c = 1.4$ mM; solvent ACN + 0.1 M NBu_4ClO_4.

can be observed and assigned to 4-cyanophenyl *tert*-butyl sulfide by comparison with an authentic sample. Thus the experiment above indicates that *(E)*-**1b** is reduced to its radical anion, whose spectrum could be recorded before further reaction to give, as already described [14], the 4-cyanophenyl *tert*-butyl sulfide.

The spectrocyclic voltammogram of *(Z)*-**1b** is presented in Fig. 6(a); Fig. 6(b), Fig. 6(c) and Fig. 6(d) present on the same potential scale the voltammogram and numerically separated absorbance–potential curves. Starting from -1.16 V vs. Fc/Fc^+ the spectrum (Fig. 6(b)) of *(Z)*-**1b** ($\lambda_{max} = 266$ nm) is stable up to approximately -1.40 V vs. Fc/Fc^+, at which potential it rapidly disappears at the expense of the spectrum of *(E)*-**1b** ($\lambda_{max} = 331$ nm); this last spectrum reaches a maximum at -1.50 V vs. Fc/Fc^+ and later decreases while the spectrum of the final product 4-cyanophenyl *tert*-butyl sulfide is recorded. Examination of Fig. 6(a) and comparison of Fig. 6(b) and Fig. 6(c) with the voltammogram of Fig. 6(d) clearly indicates that the transformation of *(Z)*-**1b** into *(E)*-**1b** occurs at a potential located approximately 150 mV in front of the peak of the cyclic voltammetric wave, i.e. at the very foot of the wave. This feature can be confirmed by examination of Fig. 7, which corresponds to a potential step from -1.12 to -1.32 V vs. Fc/Fc^+, well in front of the cyclic voltammetry peak, a potential at which the current is negligible (cf. Fig. 7(d)). Both the three-dimensional plot and the outcome reported in Fig. 7(b) and Fig. 7(c) clearly show that the stereomutation from the *(Z)*- to the *(E)*-isomer takes place at a potential (positive to the electrochemical wave) where the current in the cyclic voltammogram cannot be distinguished from the background.

These spectroelectrochemical experiments not only show a fast *(Z)* to *(E)* conversion occurring at the level of the radical anion for both **1a** and **1b**, but also that such stereomutation takes place in front of the reduction wave of both isomers, at a potential where the current flowing through the electrode cannot be distinguished from the background. This clearly indicates that the stereomutation is a very efficient electrochemically catalyzed reaction.

3.3. Fast scan rate cyclic voltammetry

Although low scan rate cyclic voltammetry does not show substantial evidence of the electrochemically catalyzed *(Z)*-**1a,b** to *(E)*-**1a,b** stereomutation, spectroelectro-

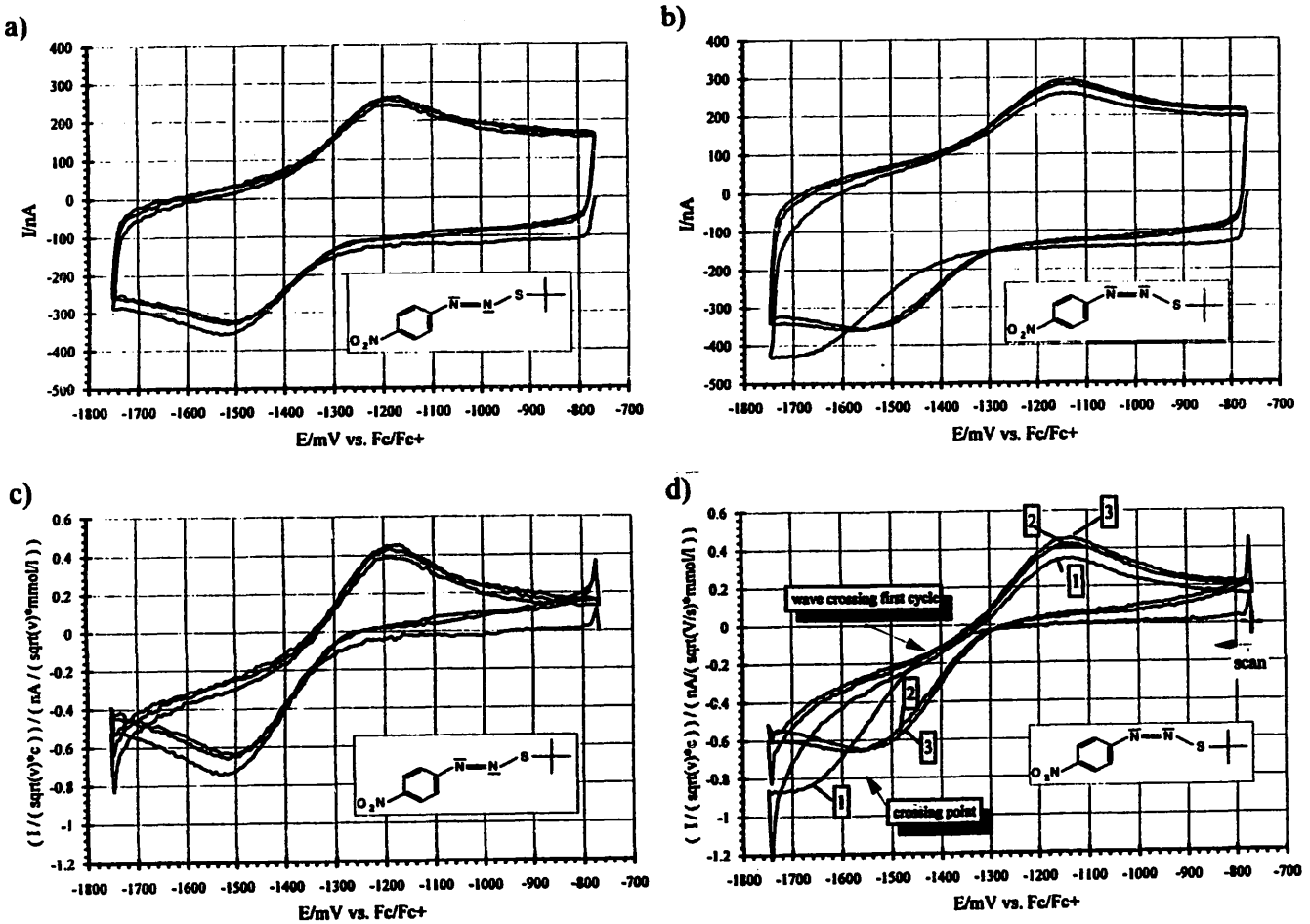

Fig. 8. Cyclic voltammograms on a 10 μm diameter gold disk electrode (three cycles) of (a) *(E)*-**1a** and (b) *(Z)*-**1a**. $c = 3$ mM, $v = 12\,000$ V s^{-1} and (c) and (d) the normalized and background corrected cyclic voltammograms of (a) and (b) respectively. Solvent ACN + NBu_4ClO_4.

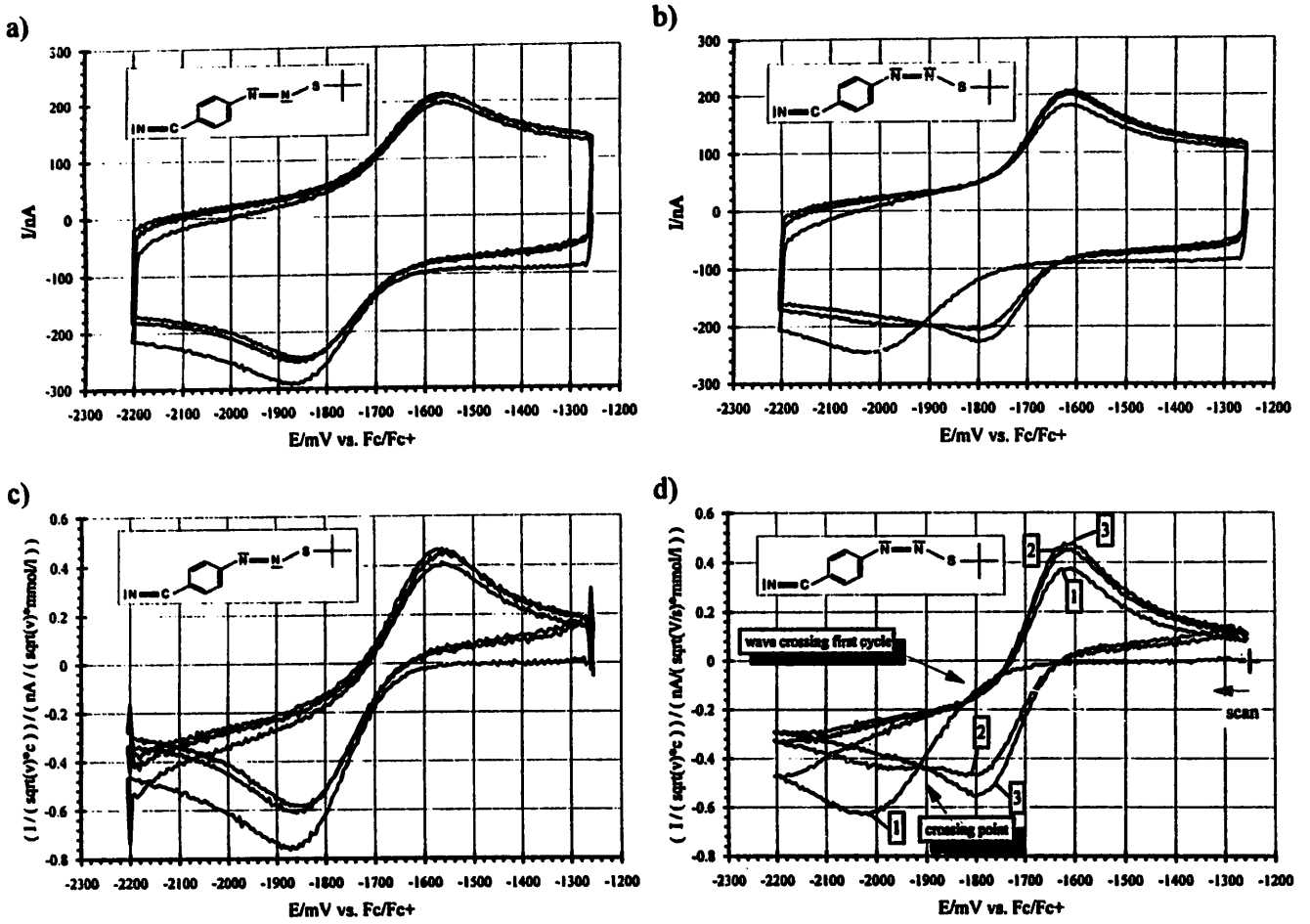

Fig. 9. Cyclic voltammograms on a 10 μm diameter gold disk electrode (three cycles) of (a) 2.8 mM *(E)*-**1b** at $v = 9100\,V\,s^{-1}$ and (b) *(Z)*-**1a**, $c = 2.6\,mM$, $v = 12000\,V\,s^{-1}$ and (c) and (d) the normalized and background corrected cyclic voltammograms of (a) and (b) respectively. Solvent ACN + NBu_4ClO_4.

chemistry points to a fast isomerization at the level of the radical anion. We therefore examined the high scan rate cyclic voltammetry of both **1a** and **1b**.

On a 10 μm diameter gold electrode at a scan rate of $12000\,V\,s^{-1}$ [22], *(E)*-**1a** presents (Fig. 8(a)), as expected, a reversible voltammogram and the second and third cycles superimpose on the first one; this is not the case with *(Z)*-**1a** (Fig. 8(b)), where the cathodic peaks of the second and third cycles are located approximately 160 mV positive to that of the first cycle, while the anodic peaks of the three cycles occur at the same potential. Fig. 8(c) and Fig. 8(d) illustrate the above results for voltammograms where

Table 1
Electrochemical data for **1a** and **1b** [a]

	$E^\circ(E)$/ V vs. SCE	$E^\circ(E)$/ V vs. Fc/Fc^+	$k_s(E)$/ $cm\,s^{-1}$	$\alpha(E)$	$E^{\circ\prime}(Z)$/ V vs. SCE [c]	$E^{\circ\prime}(E)$/ V vs. Fc/Fc^+	$k_s^*(Z)$/ $cm\,s^{-1}$ [d]	$\alpha(Z)$	k_6/s^{-1}
(E)-**1a**	-0.91_8	-1.32_3	0.21	0.46					
(Z)-**1a**	[b]	[b]			−1.12	−1.53	0.02	0.32	6.3×10^6
(E)-**1b**	-1.29_2	-1.69_7	0.46	0.44					
(Z)-**1b**	[b]	[b]			−1.16	−1.96	0.06	0.32	4.0×10^6

[a] Obtained from the non-linear fit of cyclic voltammograms ($1000 < v < 12000\,V\,s^{-1}$) at a 10 μm diameter gold disc electrode assuming a diffusion controlled rate constant for backward reaction (7) [e].

[b] From the simulation of the voltammograms of *(E)*-**1a** and *(E)*-**1b** it is possible to obtain the electrochemical data for *(Z)*-**1a** and *(Z)*-**1b**, i.e. (i) E°, respectively −0.93 and −1.29 V vs. SCE and −1.33 and −1.70 V vs. Fc/Fc^+; (ii) k_s, respectively 0.29 and $1.66\,cm\,s^{-1}$; (iii) α, respectively 0.44 and 0.42.

[c] $E^{\circ\prime}(Z) = E(Z) - (RT/\alpha(Z)F)\ln(k_s(E)/k_s(Z))$.

[d] $k_s^*(Z) = k_s(Z)\exp(\alpha_z F/RT)(E^\circ(E) - E^\circ(Z))$.

[e] $D = 1.9$, 2.0, 2.1 and $1.9 \times 10^{-5}\,cm^2\,s^{-1}$ for *(E)*-**1a**, *(Z)*-**1a**, *(E)*-**1b**, *(Z)*-**1b** respectively.

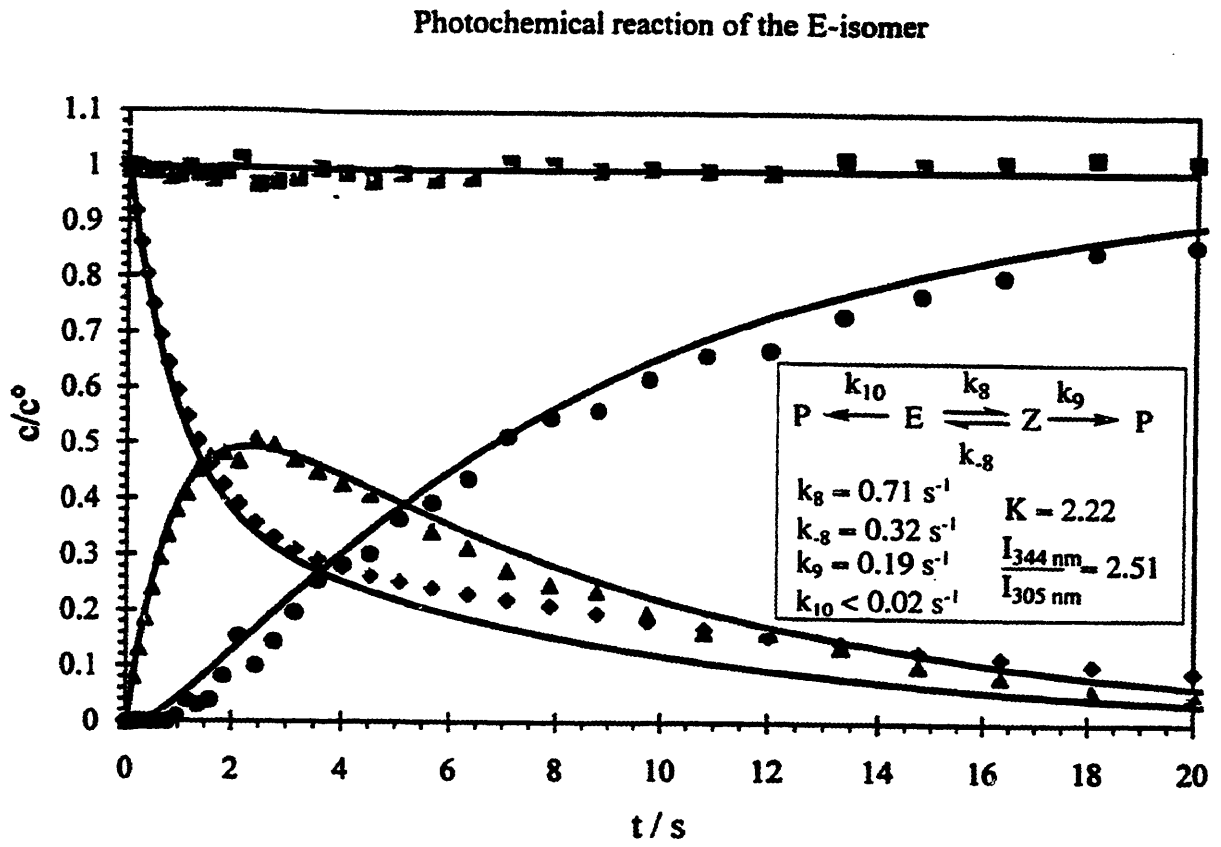

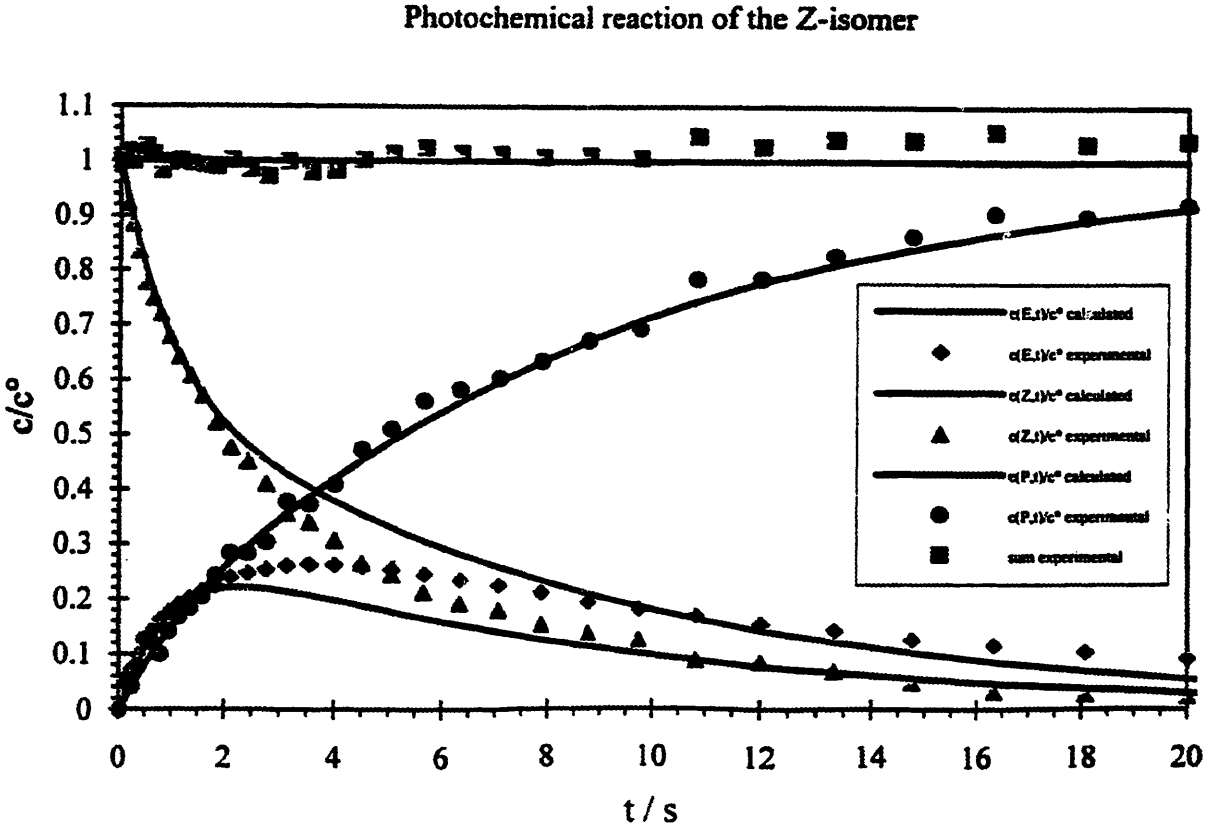

Fig. 10. Experimental and calculated normalized concentration–time curves for (*E*)-**1a** and (*Z*)-**1a** upon irradiation with a xenon lamp. $c = 2.2$ mM in ACN.

the baseline has been subtracted. On the first cycle of (Z)-**1a** one observes the crossing of the negative and positive traces, an outcome which is indicative of an electrochemically induced reaction where the standard potential of the product is positive to that of the reactant [20]. Therefore, one can expect $E^{\circ}_{(E)\text{-}\mathbf{1a}/(E)\text{-}\mathbf{1a}^{\cdot-}} > E^{\circ}_{(Z)\text{-}\mathbf{1a}/(Z)\text{-}\mathbf{1a}^{\cdot-}}$.

On a millimetric glassy carbon electrode the peak potential of both isomers of **1b** shifts by $30\,mV/\log_{10}(v)$ from $100\,mV\,s^{-1}$ to $200\,V\,s^{-1}$, indicating that the fast electron transfer is followed by a first order reaction [23]. Increasing the scan rate and using a 10 μm diameter gold disk electrode (Fig. 9) the voltammogram of (E)-**1b** becomes reversible. Under these conditions the cathodic peaks of the second and third cycle of (Z)-**1b** (Fig. 9(b) and Fig. 9(d)) are located approximately 220 mV positive to that of the first cycle; the position of such cathodic peaks is somehow shifted with respect to the same peak in Fig. 9(a); however the E° value of the (E)-isomer measured from Fig. 9(a) or Fig. 9(b) as the midpoint between the anodic and cathodic peaks is found to be the same starting from both (Z)- and (E)-isomers (see Table 1). The background corrected curve shows, as for (Z)-**1a**, crossing between the negative and positive traces of the first cycle.

These high scan rate voltammograms can be interpreted in the following way: in the case of the (E)-isomers, one observes a simple reversible system. For the (Z)-isomer the cathodic peak observed on the first cycle can be assigned to the (Z)-isomer. As to the anodic peaks and cathodic peaks of the second and third cycles, observed at more positive potentials, they pertain to the (E)-isomer formed upon stereomutation during the first scan. Observation of trace crossing on the first cycle supports the electrocatalytic character of the reaction already observed by spectroelectrochemistry.

3.4. Photochemical isomerization

Previous experiments had shown that it is possible [4,24,25] to isomerize (E)-azosulfides to (Z)-azosulfides under diffuse daylight, the reverse reaction being of thermal nature [26,27]. This is similar to the extensively investigated photoisomerization of azobenzenes which takes place from $n\pi^*$ or $\pi\pi^*$ bands [28,29]; the generally more stable (E)-form is isomerized to the less stable (Z)-form upon irradiation with UV or visible light to yield a photostationary composition which is wavelength and temperature dependent. There is no evidence of emission from the photoexcited states, indicating that the photochemical process is entirely efficient [30]. It was therefore important to find out whether such (E) to (Z) isomerization, which is opposite to the electrochemically induced isomerization, could take place under our experimental conditions.

Using the full power of the xenon lamp of the spectrophotometer it is possible to trigger the isomerization of **1a** and to follow the reaction by recording the spectra as a function of time and then to separate numerically the spectra of substrate and product. The ratio of intensities of the Xe lamp $I_{(344\,nm)}/I_{(305\,nm)}$, corresponding to the absorption maximum of the (E)- and (Z)-isomer respectively, is equal to 2.51. Under such conditions it is possible to observe the interconversion of both isomers as shown in Fig. 10. Starting from (E)-**1a** (Fig. 10(a)), a steady decrease of this isomer is observed while the (Z)-isomer increases, the latter goes through a maximum and then decreases. After an induction period of approximately 2 s the product of the photochemical reaction, i.e. 4-nitrophenyl *tert*-butyl sulfide, is formed, reaching a 90% yield after 20 s. The separation indicates that no side-product is formed. The same behavior is observed (Fig. 10(b)) starting from (Z)-**1a** with the difference that the product starts to form immediately upon irradiation.

It was possible to obtain a reasonable fit of the experimental curves of Fig. 10 (for both isomers) with calculated curves for a simple mechanism which involves an equilibrium between the two isomers (see Appendix B):

$$P \xleftarrow{k_{10}} E \underset{k_{-8}}{\overset{k_8}{\rightleftharpoons}} Z \xrightarrow{k_9} P$$

and to determine $k_8 = 0.71\,s^{-1}$, $k_{-8} = 0.32\,s^{-1}$, $K_8 = 2.22$, $k_9 = 0.19\,s^{-1}$ and $k_{10} < 0.02\,s^{-1}$. In order to minimize this (E) to (Z) isomerization during the spectroelectrochemical experiments, the intensity of the light was reduced to a minimum and the shutter was closed between each recording of spectra. However, this photochemical reaction is probably responsible for the formation of a small amount of (Z)-isomer during the measurements concerning (E)-**1a** (Fig. 3), as no trace of the (Z)-isomer can be detected by NMR spectroscopy in the pure starting material.

4. Discussion

Let us first consider the (E)-isomers. Although the radical anion of (E)-**1a** is stable on the timescale of slow scan rate cyclic voltammetry, the rate constant for its decomposition can be measured by spectroelectrochemistry from the decay of its spectrum: $k_{2[(E)\text{-}\mathbf{1a}]} = 7.5 \times 10^{-3}\,s^{-1}$. For (E)-**1b** radical anion the cleavage rate constant has previously been measured [14] as $k_{2[(E)\text{-}\mathbf{1b}]} = 1000\,s^{-1}$ from a plot of the peak potential against the logarithm of the scan rate [23]; the spectroelectrochemical analysis herein provides a value of $k_{2[(E)\text{-}\mathbf{1b}]} = 550\,s^{-1}$ and a reasonable fitting of the voltammetric curves [31] yields $k_{2[(E)\text{-}\mathbf{1b}]} = 300\,s^{-1}$. The fair agreement between the last two values indicates the previous estimation [14] as somewhat too high, likely due to the involvement of slow heterogeneous electron transfer.

As concerns the (Z)-isomers, the obtained results can be rationalized through a chain process triggered by the formation (Eq. (5)) of (Z)-$\mathbf{1}^{\cdot-}$. Eqs. (6) and (7) then represent

chain propagation steps of a process where fragmentation reactions, as in Eq. (2), of both *(E)*- and *(Z)*-$\mathbf{1}^{\cdot-}$ are possible termination steps.

$$(Z)\text{-}\mathbf{1} + 1e^- \rightarrow (Z)\text{-}\mathbf{1}^{\cdot-} \quad (5)$$

$$(Z)\text{-}\mathbf{1}^{\cdot-} \rightleftharpoons (E)\text{-}\mathbf{1}^{\cdot-} \quad (6)$$

$$(E)\text{-}\mathbf{1}^{\cdot-} + (Z)\text{-}\mathbf{1} \rightleftharpoons (Z)\text{-}\mathbf{1}^{\cdot-} + (E)\text{-}\mathbf{1} \quad (7)$$

Simulation of the above mechanism and fitting of the calculated curves with the experimental voltammograms (Fig. 11) [31] provided the parameters of Table 1 (see also Appendix C). The E° value of the *(E)*-isomers can be obtained in a straightforward manner from their reversible voltammogram but also from the simulation of the voltammograms of the *(Z)*-isomers; the very close values obtained support the validity of the simulation. It is not possible to determine likewise the E° values for the *(Z)*-isomers, but only those of $E^{\circ *}(Z) = E^\circ(Z) - RT/\alpha(Z)F \ln k_s(E)/k_s(Z)$. If the heterogeneous rate constants are supposed to be equal for the two processes, then the E° value for the *(Z)*-isomer is about 200 mV more negative than that of the *(E)*-isomer, in view of the difference in cathodic peak potentials. The other interesting datum provided by these simulations is the high rate of the isomerization reaction, of the order of $10^6\ s^{-1}$.

Other relevant electrochemically catalyzed isomerizations previously reported in the literature include stereomutation around N=N double bonds induced by single electron reduction of azobenzene [15,16] and azocyclohexanes [32], as well as oxidation of azonorbornanes [33]. Cyclic voltammetry (with several cycles) has permitted to demonstrate the electrocatalytic conversion of the *(Z)*-isomer of azobenzene into the *(E)*-isomer and to differentiate between the two isomers; at a scan rate of $10\ V\ s^{-1}$ the peak of the *(Z)*-isomer is 60 mV more negative than that of the *(E)*-isomer. It was thus possible to measure the lifetime of the *(Z)*-radical anion (0.1 ms) as well as the activation energy of the reaction ($8\ kJ\ mol^{-1}$) [16]. The electrochemical isomerization around a C=C double bond has also been scrutinized in stilbenes [34–36], maleates or fumarates [37,38], thioindigo [39,40]. In every case an electrocatalytic isomerization from the *(Z)*-isomer to the *(E)*-isomer was observed.

Our results are indeed in agreement with the almost general more difficult reducibility of the *(Z)*-isomer with respect to the *(E)*-isomer, indicating a higher energy for the LUMO of the *(Z)*-isomer of approximately 0.2 eV above that of the *(E)*-isomer. Perhaps the main point which emerges from the comparison with literature data is that the isomerization of the studied arylazo *tert*-butyl sulfides

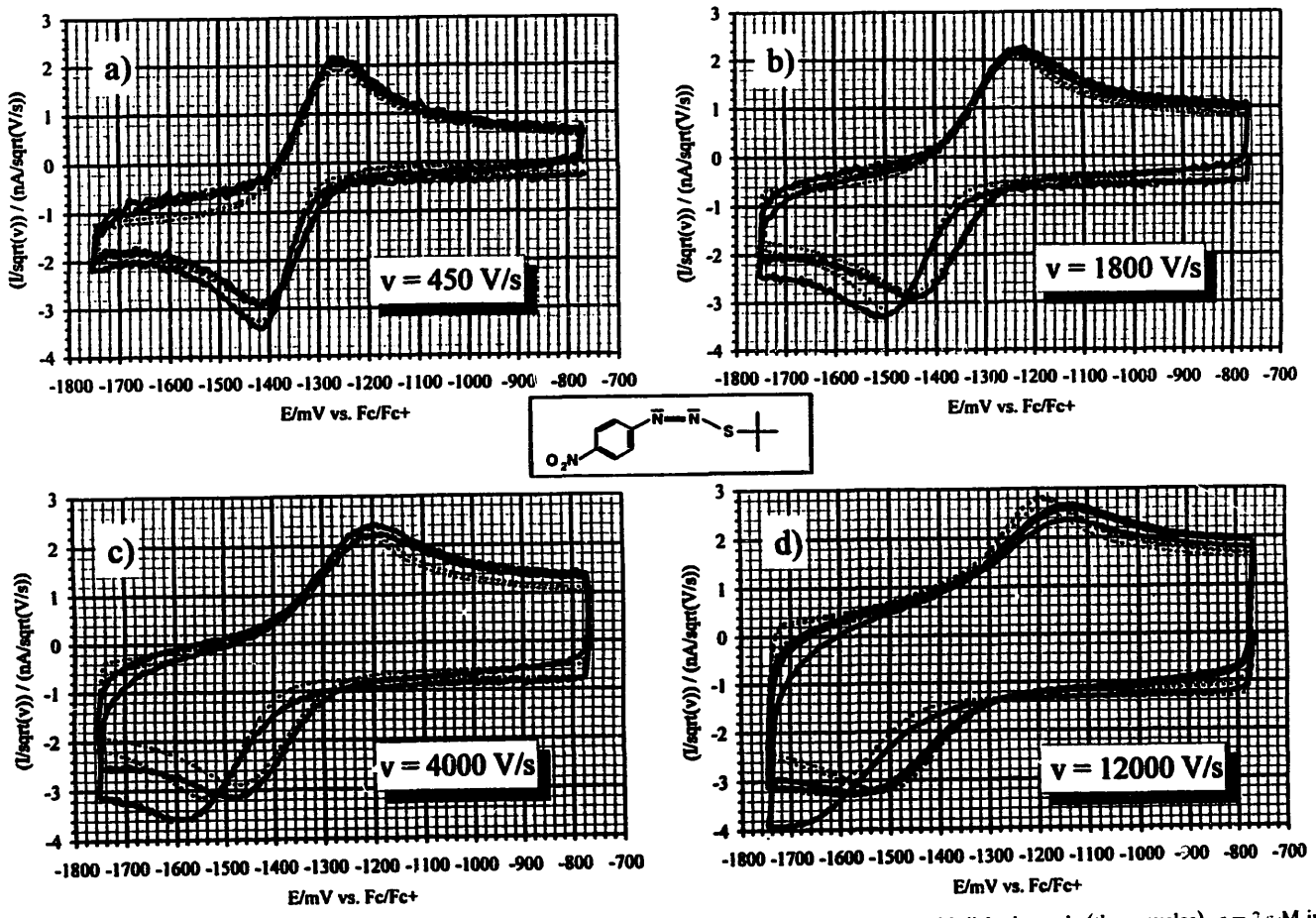

Fig. 11. Cyclic voltammograms of *(Z)*-1a simulated (· · ·) and experimental (---) on a 10 μm diameter gold disk electrode (three cycles). $c = 3$ mM in ACN + NBu_4ClO_4.

is much faster than any previously measured electrochemically induced *(Z)* ⇌ *(E)* isomerization, an outcome which should find a mechanistic rationalization. Actually, three different mechanisms have been essentially proposed for the *cis* to *trans* isomerization of azoderivatives, namely (a) twisting around the nitrogen–nitrogen bond (rotation mechanism), (b) planar variation of one or (c) both C–N–N angles. In the case of the photochemical isomerization of azobenzene, i.e. involving excited states and not radical anions, both a rotation and an inversion mechanism around the azo group have been advocated [41–43]. As to the electrochemical isomerization herein, involving a radical anion, it may be that the sulfur atom increases the rate of the planar mechanism by the involvement of its d orbitals. Following previous reports a possible way to answer the question would be to design azosulfides where the rotation mechanism is blocked [43] or to perform calculations of the activation energy of both processes [41].

In the light of the high value obtained herein ($4 \times 10^6\ s^{-1}$) for the *(Z)*- to *(E)*-**1b** stereomutation when compared with the fragmentation rate of the relevant radical anion **1b**$^{\cdot-}$ [$k_{2(E)\text{-}\mathbf{1b}}$ ca. $5 \times 10^2\ s^{-1}$], we reconsidered our previous results [14]. As reported in the Introduction, such results indicate different rates of trapping of the 4-cyanophenyl radical ensuing from fragmentation of **1b**$^{\cdot-}$ (Eq. (2)), by excess cyanide as 'external' nucleophile when starting from either *(E)*- or *(Z)*-**1b**. Actually, new measurements carried out with a different experimental procedure (see Experimental section) indicate that the data previously obtained [14] for the *(Z)*-isomer of the 4-cyanophenylazo *tert*-butyl sulfide (table VII of Ref. [14]) were erroneous possibly because of an unidentified practical mistake. The average of five independent measurements of the plateau corresponding to the maximum amount of aryl radicals trapped by the 'external' nucleophile provided a value of $84 \pm 12\%$ for *(E)*-**1b** and $86 \pm 10\%$ for *(Z)*-**1b**. These data, which are identical within experimental uncertainty, are in agreement with a fast *(Z)* ⇌ *(E)* stereomutation at the level of **1b**$^{\cdot-}$ preceding a relatively slower fragmentation of the same radical anion.

5. Conclusions

While low scan rate cyclic voltammetry does not allow us to observe any significant difference between the voltammograms of the *(E)*- and *(Z)*-isomers of **1a** and **1b**, spectroelectrochemistry shows very clearly the transformation of the *(Z)*- into the *(E)*-isomer. This isomerization is an efficient electrocatalytic reaction. Simulation of the high scan rate cyclic voltammograms permits us at the same time to ascertain the mechanism and measure a number of parameters, such as the isomerization rate itself; this is found much higher than that relevant to previously investigated azobenzenes, indicating a probable involvement of the sulfur atom in the process.

Acknowledgements

A.N. gratefully acknowledges a grant from Deutsche Forschungsgemeinschaft (DFG). M.N. and J.P. gratefully acknowledge CNR and CNRS for contributions within the frame of International Cooperation Projects. This work was partially supported by MURST (60% funds) (Italy).

Appendix A

Spectroelectrochemical determination of the decomposition rate constant of 1b$^{\cdot-}$

The separation of the overlapping UV–vis peaks (Fig. 5) of the spectroelectrochemical experiment yields the absorbance–time dependence of each species (Fig. 5(b), Fig. 5(c)). If we consider that no significant side reaction is going on, and that the reaction after the potential step can be described by A → B → C, the sum of the concentrations c_A, c_B, c_C is equal to the initial concentration c_0. Neglecting the non-linearity between the absorbance and the concentration because of the cylindrical concentration profile parallel to the light beam in the first 50 ms after the potential step, the sum of concentrations can be written as a sum of absorbances if the absorbance of each species is normalized to its absorbance for the initial concentration c_0:

$$\frac{\mathrm{Abs_A}(t)}{\mathrm{Abs_{A,c_0}}} + \frac{\mathrm{Abs_B}(t)}{\mathrm{Abs_{B,c_0}}} + \frac{\mathrm{Abs_C}(t)}{\mathrm{Abs_{C,c_0}}} = 1$$

The absorbance–time curve of each species (Fig. 5) shows that $\mathrm{Abs_{A,c_0}} = \mathrm{Abs_A}(0\,\mathrm{ms})$ and $\mathrm{Abs_{C,c_0}} = \mathrm{Abs_C}(t)$ with $t > 450$ ms. Therefore

$$\mathrm{Abs_{B,c_0}} = \frac{\mathrm{Abs_B}(t)}{1 - \dfrac{\mathrm{Abs_A}(t)}{\mathrm{Abs_{A,c_0}}} - \dfrac{\mathrm{Abs_C}(t)}{\mathrm{Abs_{C,c_0}}}}$$

at each time when $\mathrm{Abs_B}(t) > 0$. As $\mathrm{Abs_B}(t = 0) = 0$ and $\mathrm{Abs_B}(t = \infty) = 0$, and as the same conditions are fulfilled for the denominator of Eq. (1), this equation can be transformed into

$$\mathrm{Abs_{B,c_0}} = \frac{\displaystyle\int_0^\infty \mathrm{Abs_B}(t)\,\mathrm{d}t}{\displaystyle\int_0^\infty \left(1 - \frac{\mathrm{Abs_A}(t)}{\mathrm{Abs_{A,c_0}}} - \frac{\mathrm{Abs_C}(t)}{\mathrm{Abs_{C,c_0}}}\right)\mathrm{d}t}$$

The limit conditions are fulfilled at $t > 450$ ms and $\mathrm{Abs_{B,c_0}}$ can be determined from the quotient of the limit values of both integrals.

Replacing the concentrations in the simple kinetic equation

$$\frac{\mathrm{d}c_C}{\mathrm{d}t} = kc_B$$

by the normalized absorbances at the initial concentration, one obtains upon integration

$$\frac{\mathrm{Abs_C}(t)}{\mathrm{Abs_{C,c_0}}} = k\int_0^t \frac{\mathrm{Abs_B}(x)}{\mathrm{Abs_{B,c_0}}}\,\mathrm{d}x$$

and $k_{2[(E)\text{-}\mathbf{1b}]}$ can be determined. A linear plot is obtained from which the value $k_{2[(E)\text{-}\mathbf{1b}]} = 556\,\mathrm{s}^{-1}$ is measured; an error of $\pm 120\,\mathrm{s}^{-1}$ can be estimated.

Appendix B

Concentration–time curves during the photoisomerization of 1a

Assuming a reaction scheme

$$P \overset{k_{10}}{\leftarrow} E \underset{k_{-8}}{\overset{k_8}{\rightleftharpoons}} Z \overset{k_9}{\rightarrow} P$$

with $E(0)$, $Z(0)$ and $P(0)$ as initial conditions, one obtains

$$\frac{\mathrm{d}E}{\mathrm{d}t} = -(k_8 + k_{10})E + k_{-8}Z;$$

$$\frac{\mathrm{d}Z}{\mathrm{d}t} = k_8 E - (k_{-8} + k_9)Z;\quad \frac{\mathrm{d}P}{\mathrm{d}t} = k_{10}E + k_9 Z$$

The differential equation system can be solved by using a Laplace transformation, which gives a simple linear equation system

$$E(0) = (k_8 + k_{10} + s)\bar{E} + (-k_8)\bar{Z} + 0\bar{P}$$

$$Z(0) = (-k_8)\bar{E} + (k_{-8} + k_9 + s)\bar{Z} + 0\bar{P}$$

$$P(0) = -k_{10}\bar{E} + (-k_9)\bar{Z} + (+s)\bar{P}$$

The first two equations are independent of the last one; the solution yields

$$\bar{E} = \frac{E(0)(k_{-8} + k_9 + s) + Z(0)k_{-8}}{(k_8 + k_{10} + s)(k_{-8} + k_9 + s) - k_8 k_{-8}}$$

$$\bar{Z} = \frac{E(0)k_8 + Z(0)(k_8 + k_{10} + s)}{(k_8 + k_{10} + s)(k_{-8} + k_9 + s) - k_8 k_{-8}}$$

$$\bar{P} = \frac{k_{10}\bar{E} + k_9\bar{Z} + P(0)}{s}$$

the backward transformation yields

$$E(t) = \exp(\beta t)\left[\frac{\sinh(\alpha t)}{\alpha}\left[E(0)(k_{-8} + k_9 - \beta) + Z(0)k_{-8}\right] + E(0)\cosh(\alpha t)\right]$$

$$Z(t) = \exp(\beta t)\left[\frac{\sinh(\alpha t)}{\alpha}\left[E(0)(k_{-8} + k_9 - \beta) + Z(0)(k_8 + k_{10} - \beta)\right] + Z(0)\cosh(\alpha t)\right]$$

$$\alpha = \sqrt{\beta^2 - k_8 k_9 - k_{-8}k_{10} - k_9 k_{10}}$$

with

$$\beta = \frac{k_8 + k_{-8} + k_9 + k_{10}}{2}$$

The expression for the time curve of the product can be written as

$$Pt = \int_0^t k_{10}E(\tau) + k_9 Z(\tau)\,\mathrm{d}\tau + P(0)$$

Appendix C

Determination of the electrochemical parameters of the electrochemically induced *(Z)* to *(E)* isomerization by non-linear regression analysis using Digisim V2.0

The electrochemical *(Z)* to *(E)* isomerization can be described by the following scheme:

$E + e^- \rightleftharpoons E^{\cdot -}$	$E°(E)$, $\alpha(E)$, $k_{s,app}(E)$
$Z + e^- \rightleftharpoons Z^{\cdot -}$	$E°(Z)$, $\alpha(Z)$, $k_{s,app}(Z)$
$Z^{\cdot -} \rightarrow E^{\cdot -}$	k_6
$Z^{\cdot -} + E \rightleftharpoons Z + E^{\cdot -}$	k_7, k_{-7}

with the nine parameters given in the scheme, an additional general diffusion constant for all species and taking in account that $E°(E) - E°(Z) = RT/F \ln k_7/k_{-7}$, at least nine parameters have to be determined. The parameters of the charge transfer of the *(E)*-isomer can be determined from the voltammograms of the *(E)*-isomer but also from the second and third cycles on the voltammograms of the *(Z)*-isomer when all the $(Z)/(Z^{\cdot -})$ couple has been replaced by the $(E)/(E^{\cdot -})$ couple in the diffusion layer. If $E°(E) > E°(Z)$ then $k_7 > k_{-7}$ and the concentration of $Z^{\cdot -}$ tends toward zero, the same situation occurs if the isomerization is fast. In the case of both **1a** and **1b**, the reversibility of the *(Z)*-isomer cannot be observed up to $4 \times 10^4\,\mathrm{V\,s}^{-1}$ and it is therefore not possible to determine $E°(Z)$. Under such conditions, where the concentration of $(Z^{\cdot -})$ tends toward zero, the partial current of the *(Z)*-isomer can be written as

$$i(Z) = k_s^*(Z)FSc(Z)_{y=0}\exp\left[-\frac{\alpha(Z)F}{RT}\right]E;$$

$$k_s^* = k_{s,app}(Z)\exp\left[-\frac{\alpha(Z)F}{RT}\right]E°(Z)$$

and the current depends only on k^* instead of the two parameters $E°(Z)$ and $k_{s,app}(Z)$, which reduces to six the number of parameters and a common diffusion coefficient. Assuming that k_7 is at the diffusion limit and normalizing $k_s(Z)$ to $k_s(E)$, it is possible to define a potential

$$E°^*(Z) = E(Z) - \frac{RT}{\alpha(Z)F}\ln\frac{k_s(E)}{k_s(Z)}$$

which is equal to $E°(Z)$ if $k_s(E)$ is equal to $k_s(Z)$. Con-

versely, the normalization of the potential between $E°(E)$ and $E°(Z)$:

$$k_s^*(Z) = k_s(Z)\exp\left[\frac{\alpha_- F}{RT}\right]\left[E°(E) - E°(Z)\right]$$

These relations are used to present the results of the non-linear fit of the cyclic voltammograms shown in Table 1, and it can be seen that the simulated voltammograms are identical when $E°(Z)$ is changed keeping k^* constant.

References

[1] G. Petrillo, M. Novi, G. Garbarino and C. Dell'Erba, Tetrahedron, 42 (1986) 4007.
[2] G. Petrillo, M. Novi, G. Garbarino and C. Dell'Erba, Tetrahedron, 43 (1987) 4625.
[3] G. Petrillo, M. Novi, C. Tavani and G. Berta, Tetrahedron, 46 (1990) 7977.
[4] C. Dell'Erba, M. Novi, G. Petrillo, C. Tavani and P. Bellandi, Tetrahedron, 47 (1991) 333.
[5] C. Dell'Erba, M. Novi, G. Petrillo and C. Tavani, Tetrahedron, 48 (1992) 325.
[6] C. Dell'Erba, M. Novi, G. Petrillo and C. Tavani, Tetrahedron, 49 (1993) 235.
[7] C. Dell'Erba, M. Novi, G. Petrillo and C. Tavani, Tetrahedron, 50 (1994) 3529.
[8] J.F. Bunnett, Acc. Chem. Res., 11 (1978) 413.
[9] R.A. Rossi and R.H. Rossi, Aromatic Nucleophilic Substitution by the $S_{RN}1$ Mechanism, ACS Monograph 178, American Chemical Society, Washington, DC, 1983.
[10] J. Pinson and J.-M. Savéant, J. Chem. Soc., Chem. Commun., (1974) 933.
[11] J.-M. Savéant, Acc. Chem. Res., 13 (1980) 123.
[12] J.-M. Savéant, Adv. Phys. Org. Chem., 26 (1990) 1.
[13] J. Pinson and J.-M. Savéant, in R.D. Little and N.L. Weinberg (Eds.), Electroorganic Synthesis, Marcel Dekker, New York, 1991, p. 29.
[14] C. Dell'Erba, A. Houmam, M. Novi, G. Petrillo and J. Pinson, J. Org. Chem., 58 (1993) 2670.
[15] G. Klopman and N. Doddapaneni, J. Phys. Chem., 78 (1974) 1825.
[16] E. Laviron and Y. Mugnier, J. Electroanal. Chem., 93 (1978) 69.
[17] A. Neudeck and L. Dunsch, J. Electroanal. Chem., 370 (1994) 17.
[18] A. Neudeck and L. Dunsch, J. Electroanal. Chem., 386 (1995) 138.
[19] A. Neudeck and L. Dunsch, Electrochim. Acta, 40 (1995) 1427.
[20] C. Amatore, J. Pinson, J.-M. Savéant and A. Thiébault, J. Electroanal. Chem., 107 (1980) 59.
[21] C. Dell'Erba, A. Houmam, N. Morin, M. Novi, G. Petrillo, J. Pinson and C. Rolando, J. Org. Chem., 61 (1996) 1331.
[22] C.P. Andrieux, D. Garreau, P. Hapiot, J. Pinson and J.-M. Savéant, J. Electroanal. Chem., 243 (1988) 321.
[23] C.P. Andrieux and J.-M. Savéant, Electrochemical reactions, in C.F. Bernasconi (Ed.), Investigations of Rates and Mechanisms of Reaction, Techniques of Chemistry, Vol. VI:4E, Wiley, New York, 1986, pp. 305–390.
[24] H. van Zwet and E.C. Kooyman, Rec. Trav. Chim. Pays-Bas, 86 (1967) 993.
[25] L.K.H. van Beek, J.R.G.C.M. van Beek, J. Boven and C.J. Schoot, J. Org. Chem., 36 (1971) 2195.
[26] J. Broken-Zijp and H. van der Bogaert, Tetrahedron, 29 (1973) 4169.
[27] J. Broken-Zijp and H. van der Bogaert, Tetrahedron Lett., (1974) 249.
[28] J. Maack, R.C. Ahuja and H. Tachibana, J. Phys. Chem., 99 (1995) 9210 and references cited therein.
[29] R.G. Compton, R.G. Wellington, D. Bethell, P. Lederer and D.M. O'Hare, J. Electroanal. Chem., 322 (1992) 183.
[30] G. Sudesh Kumar and D.C. Neckers, Chem. Rev., 89 (1989) 1915 and references cited therein.
[31] M. Rudolph and S.W. Feldberg, Digisim 2.0, Cyclic Voltammetric Simulator for Windows, Bioanalytical Systems Inc.
[32] C. Degrand and G. Belot, Electrochim. Acta, 21 (1978) 71.
[33] G. Gesheidt, A. Lamprecht, J. Heinze, B. Schüler, M. Schmittel, S. Kiau and C. Rüchardt, Helv. Chim. Acta, 75 (1992) 1607.
[34] R. Dietz and M.E. Peover, Discuss. Faraday Soc., 45 (1968) 154.
[35] B.S. Jensen, R. Lines, P. Pasbcrg and V.D. Parker, Acta Chem. Scand., B31 (1977) 707.
[36] C.K. Chien, H.C. Wang, M. Swarc, A.J. Bard and K. Itaya, J. Am. Chem. Soc., 102 (1980) 3100.
[37] A.J. Bard, V.J. Puglisi, J.V. Kenkel and A. Lomax, Faraday Discuss. Chem. Soc., 56 (1973) 353.
[38] L.S. Yeh and A.J. Bard, J. Electrochem. Soc., 124 (1977) 189.
[39] L.S. Yeh and A.J. Bard, J. Electroanal. Chem., 70 (1976) 157.
[40] L.S. Yeh and A.J. Bard, J. Electroanal. Chem., 81 (1977) 333.
[41] S. Monti, G. Orlandi and P. Palmieri, Chem. Phys, 71 (1982) 87.
[42] H. Rau, J. Photochem., 26 (1984) 221.
[43] H. Rau and E. Lüddecke, J. Am. Chem. Soc., 104 (1982) 1616.